DOI: 10.1002/((please add manuscript number))
Article type: Communication

Title: A needle-type microrobot for targeted drug delivery by affixing to a microtissue

*Seungmin Lee, Jin-young Kim, Junyoung Kim, Ali Kafash Hoshiar, Jongeon Park, Sunkey Lee, Jonghyun Kim, Salvador Pané, Bradley J. Nelson, and Hongsoo Choi**

S. Lee, Dr. J. Kim, J. Kim, J. Park, S. Lee, Prof. J. Kim, Prof. H. Choi*
Department of Robotics Engineering, DGIST-ETH Microrobot Research Center
Daegu-Gyeongbuk Institute of Science & Technology (DGIST)
333, Techno jungang-daero, Hyeonpung-eup, Dalseong-Gun, Daegu, 42988, Republic of Korea
E-mail: mems@dgist.ac.kr

Dr. A. K. Hoshiar
School of Computer Science and Electronic Engineering,
University of Essex
Colchester, CO4 3SQ, United Kingdom

Dr. S. Pané, Prof. B. J. Nelson,
Institute of Robotics and Intelligent Systems
ETH Zurich, Zurich, CH-8092, Switzerland

Keywords: Microrobot; magnetic manipulation; drug delivery; targeted delivery; fixation

Abstract:

A needle-type microrobot (MR) for targeted drug delivery was developed to stably deliver drugs to a target microtissue (MT) for a given period time without the need for an external force after affixing. The MRs were fabricated by 3D laser lithography and Ni/TiO_2 layers were coated by physical vapor deposition. The translational velocity of the MR is 714 μm/s at 20 mT and affixed to the target MT under the control of a rotating magnetic field. The manipulability of the MR was shown by using both manual and automatic controls. Finally, drug release from the paclitaxel (PTX)-loaded MR was characterized to determine the efficiency of targeted drug delivery. This study demonstrated the utility of the proposed needle-type MR for targeted drug delivery to MT with various flow rates in vitro physiological fluidic environments.

Chemotherapy is used along with irradiation and surgery in the treatment of various cancers. Due to its efficacy in cancer,[1] there is a great deal of ongoing research on chemotherapy drugs, ranging from cytotoxic to targeted anticancer drugs.[2] However, adverse drug reactions (ADRs), such as hair loss, nausea, vomiting, and loss of appetite, remain problematic.[3] Therefore, it is important to ensure that appropriate amounts of chemotherapeutic drugs are delivered accurately to the lesion to minimize side effects. The use of medical microrobots (MRs) has recently emerged as a promising means of achieving targeted drug delivery; their tiny size and remote control have great potential for minimally invasive surgery.

A number of MRs of various shapes have been developed, including helical-,[4] scaffold-,[5] ciliary-,[6] and capsule-type MRs,[7] for drug and cell delivery. Other types of MRs have also been developed for delivery of cells,[4e, 5, 8] drugs,[9] genes,[4d] surgery,[10] scanning,[11] and actuation[12] in various applications. To date, most MR research has focused on their fabrication, propulsion mechanisms,[6] and applications. Different magnetic fields are used to induce MRs to swim in a fluidic environment with a low Reynolds number. However, previously developed MRs were difficult to fix in a position for long-term targeted drug delivery without a magnetic field. They could be fixed at the lesion but were susceptible to being flushed away from the target area by body fluids. To avoid this, an external magnetic field should be continuously applied to the MR to hold it in the position after delivery. However, continuous long exposure to a magnetic field may have many technical issues and adverse effects on human health.[13] To overcome these limitations, we propose a needle-type three-dimensional (3D) MR that can be fixed at a target position to stably deliver drugs to the target for a given period time without the need for an external force after affixing. Figure 1a shows a conceptual schematic of targeted drug delivery by the needle-type MR, which can be fixed in position at the selected target tissue. First, the drug-loaded needle-type MR approaches

the target microtissue (MT) by swimming in a corkscrew motion with magnetic torque (T_m) under a rotating magnetic field (RMF), described as follows:

$$\boldsymbol{T_m} = \boldsymbol{v}\boldsymbol{M} \times \boldsymbol{B} \quad \textbf{(1)}$$

where $\boldsymbol{v}$ and $\boldsymbol{M}$ are the volume and magnetization of a magnetic object, respectively, and $\boldsymbol{B}$ is the external magnetic field.[14] The magnetic torque is related to the step-out frequency, which allows for keeping the MR in sync with the external magnetic field. Therefore, the maximum velocity and frequency of the rotating MR can be controlled by adjusting the magnitude and frequency of the RMF; the higher the translation velocity of the MR, the easier the needle-type MR can affix to the target MT. As shown in Figure 1b, the needle-type MR consists of a needle (50 μm in length) at the front, to spear the target microtissue, and a screw part (250 μm in length, 80 μm in diameter from the front view) to generate corkscrew motion under the RMF. The needle-type MR has a 3D scaffold structure over the whole body, to increase the surface area and payload of drugs. The porous structure also allows adherence to cells for targeted cell delivery.

Figure 1c illustrates the fabrication procedures of the needle-type MR. First, the basal body of the MR was formed using a two-photon polymerization (TPP) 3D laser lithography system (Photonic Professional GT; Nanoscribe GmbH, Eggenstein-Leopoldshafen, Germany). Next, nickel (Ni) and titanium oxide (TiO_2) layers were deposited on the surface of the MR by physical vapor deposition (PVD), for magnetic manipulation and to ensure biocompatibility, respectively. Figure 1d, e shows scanning electron microscopy (SEM) images of the fabricated needle-type MRs. Multiple MRs were fabricated on glass substrates. To increase the drug loading capacity, the 3D porous part was formed on both the surface and the inside of the MR.

The needle-type MR was manipulated by an external magnetic actuation (EMA) system used in our previous work.[7, 15] The translational velocity of the MR was measured as a function of RMF frequency, with magnetic intensities of 10 and 20 mT. As shown in Figure 2a,

translational velocity increased with the frequency of RMF at both 10 and 20 mT. The maximum velocity was 714 μm/s with 20 mT at 18 Hz but decreased markedly after a step-out frequency of 18 Hz. Wobbling motion was also observed above the step-out frequency due to insufficient magnetic torque and it was dependent on the magnetization of the MR, the friction and the magnetic intensity.[16]

Fixation pressure measurement has proven difficult at the microscale. To understand the characteristics of the needle-type MR for affixing to a HCT116 MT, a finite element (FE) model was developed using the structural mechanics module of COMSOL Multiphysics (v. 5.4; COMSOL AB, Stockholm, Sweden). Furthermore, two analytical models (Hertz and Johnson-Kendall-Roberts (JKR)) were used to predict the behavior.[17] The calculations revealed that the maximum fixation pressure was about 0.64 kPa in the JKR model, and about 0.82 kPa in the COMSOL model (Figure 2b).

Two methods were used to manipulate the MR: manual control and automatic control. The needle-type MR was maneuvered to be affixed to the target MT (Figure 2c). As shown in Figure 2d (i), manual control was implemented under an RMF that could be adjusted with a joystick. Despite the simplicity of the method, it took about 1 minute to affix the MR to the MT. Therefore, we developed a feedback control scheme for automatic control of the MR, to allow for rapid and accurate control of the MR.[18] By analyzing the position and orientation errors of the MR, the control scheme ensured appropriate rotational frequency and orientation of the RMF. The rotational frequency was controlled to regulate the positional error between the MR and the target MT, and the rotational axis orientation was controlled to adjust the approach direction of the MR to the MT. Moreover, control of the rotational frequency was robust to uncertainties in the time delay estimation.[18] The details are shown in Figure S1.[18] Figure 2d (ii) illustrates the manipulability of the MR under automatic control. Compared to Figure 2d (i), it shows markedly improved performance under automatic control compared to manual

control. The initial conditions in both cases were identical, but the time for fixation under automatic control was significantly shorter (7 s) than that under manual control (55 s). Furthermore, the trajectory under automatic control was much shorter and simpler than that under manual control, so the fixation accuracy of the MR to the MT could also be improved.

To demonstrate the flow resistance of the MR, various flow rates were generated in a microchannel environment using a syringe pump (NE-300; New Era Pump Systems, Inc., New York, NY, USA) (Figure S3). As the results, fixation of the MR to the MT allowed the MR to withstand higher flow rates than under unfixed condition (see Figure S4 for more details). As shown schematically in Figure S5 (e), the height of the perfusion channel was lower than the diameter of the MT. Therefore, only the MR was flushed away to the flowing direction of the medium with flow rate over 40 μl/min (flow speed: 80 mm/s, Figure S4a). On the other hand, the MT was deformed in the perfusion channel and flushed with the MR at a flow rate around 240 μl/min. (flow speed: 480 mm/, Figure S4b). As some references, the flow rates are 300 and 100 mm/s in the vena cava and in the small arteriole, respectively.[14]

After affixing to the MT, the paclitaxel (PTX, product no. P3456; Sigma-Aldrich, St. Louis, MO, USA)-loaded needle-type MR was incubated in an MT culture microchamber, which is subject to mechanical force, to investigate not only targeted drug delivery to the MT but also the stability of the fixation against mechanical force. The needle-type MR was coated with the anticancer drug PTX by hydrogen bonding.[19] The experiment was performed in the MT culture microchamber, which has a tilting platform driven by a 1 Hz motor (Figure S5). The efficiency of targeted drug delivery to the HCT116 MTs was analyzed by inverted microscopy (Axio Observer Z1; Carl Zeiss, Oberkochen, Germany) using a live – dead cell imaging kit (488/570) (R37601; Thermo Fisher Scientific, Waltham, MA, USA) for bright and fluorescence field images as shown in Figure 3a. The merged images are shown 48 hours after drug delivery. For the groups without PTX (-MR/-PTX and +MR/-PTX), the diameter of the

MT was relatively increased compared to the other group (+MR/+PTX). The MR for +MR/-PTX group gradually merged with the MT, while the MT to which the drug was delivered from the MR (+MR/+PTX) became smaller. In qualitative analysis, a lot of red fluorescence intensity was shown in the +MR/+PTX group indicating that the HCT116 cells were dead due to the drug-induced effect. In quantitative analysis, relative diameter of MT in drug-induced case (+MR/+PTX) was about 1.2 times with respect to DIV0 (Figure 3b) which is smaller compared to 1.6 for +MR/-PTX and 1.52 for -MR/-PTX. In addition, the ATP (adenosine triphosphate) contents of the HCT116 MT decreased to approximately 40% with drug delivery (Figure 3c). These results demonstrated the potential of the needle-type MR to improve targeted drug delivery performance with a certain level of flow.

In conclusion, we developed a needle-type MR for targeted drug delivery, where the needle part allows the MR to affix to the MT. The MRs were fabricated by 3D laser lithography and coated by physical vapor deposition. The translational velocity of the MR is 714 μm/s at 20 mT and affixed to the target MT under the control of an RMF. Moreover, the manipulability of the MR was shown by using both manual and automatic controls. Finally, drug release from the PTX-loaded MR was characterized to determine the efficiency of targeted drug delivery. This study demonstrated the utility of the proposed needle-type MR for targeted drug delivery to MT with various flow rates in vitro physiological fluidic environments.

Experimental Section

Fabrication of the needle-type MR: The MR was fabricated using a TPP system. The glass substrate (25 × 25 mm) was prepared and cleaned by ultrasonication in isopropyl alcohol (IPA). Photoresist (IP-S, 50–100 μl; Nanoscribe GmbH) was drop-cast onto the glass substrate, which was inserted prior to laser writing by the TPP system. The writing conditions were as follows: scaled laser power, 100%; and average scan speed, 100,000 μm s^{-1}. After writing, the

substrate was developed in SU-8 developer for 5–10 minutes and rinsed with deionized (DI) water. A Ni (255 nm)/TiO_2 (20 nm) layer was deposited on the MR by a sputtering system. Finally, the fabricated substrates were heat-treated for 30 minutes at 100°C.

Magnetic manipulation: A single needle-type MR was detached from the substrate using a syringe tip. For magnetic actuation, the MR (in DI water) was manipulated under an external RMF of 1–18 Hz at 10 and 20 mT using a magnetic steering system (MiniMag; Aeon Scientific, Zurich, Switzerland). To evaluate the MR speed, videos were taken at 15 fps using a charge-coupled device (CCD) camera (GRAS-50S5C-C; Point Grey Research Inc., Richmond, BC, Canada) integrated with the magnetic steering system. The translational speed was determined by analyzing the videos, which were generated from time-lapse images.

Drug coating: The MR was coated with PTX by hydrogen bonding[19] to evaluate targeted drug delivery performance to HCT116 MT. A high-concentration stock solution was prepared with 100% EtOH, and 3 μl of the solution was dropped onto the glass substrate directly and allowed to evaporate to coat the MR.

Fabrication and cultivation: Tumor MT was prepared using human colon cancer (HCT116) cells purchased from the Korean Cell Line Bank (KCLB, Cancer Research Institute, Seoul National University College of Medicine, Seoul, South Korea). The HCT116 cells were seeded at a concentration of 100 cells/100 μl in U-bottomed 96-well plates (Thermo Fisher Scientific). The cell culture medium consisted of RPMI 1640 (Thermo Fisher Scientific) containing 10% fetal bovine serum (FBS; Sigma-Aldrich), 100 g/ml penicillin, and 10 g/ml streptomycin. For cell aggregation, the incubation conditions were 37°C, 5 % CO_2, and > 90 % humidity for 4 days. The spherical HCT116 MT were about 300 μm in diameter.

Hydrodynamic resistance: Various flow rates were generated in the microchannel environment by a syringe pump (NE-300; New Era Pump Systems, Inc.). In the non-fixed state, the flow rates were controlled from 1–40 μl/min until the MRs were flushed out from the chamber. The

flow rates were increased in increments of 10 μl/min, from 40–240 μl/min; all flow rates were maintained for 2 minutes. The MTs were observed under an inverted microscope (Observer Z1; Carl Zeiss) with a 10× objective lens in bright-field mode.

Drug delivery to MTs from the fixed needle-type MR: To evaluate drug release performance, microchambers were prepared on a tilting platform in an incubator. The platform tilting was increased to 40° so that the MR moved from one side of the chamber to the other side within 1 s. The experiments were performed over 48 hours in the control group and the two experiment groups (w/o drug and w/ drug).

HCT116 MT viability assay: The HCT116 MT was placed into the microchannel platform and observed using an inverted microscope (Lionheart LX; BioTek, Winooski, VT, USA) with a 10× objective lens in bright-field mode. For determination of cell viability, live cells were stained with calcein AM (ex/em 488 nm/515 nm; Thermo Fisher Scientific). Also, a luminescence-based ATP assay (CellTiter-Glo; Promega Corp., Madison, WI, USA) was conducted using the luminescence measurement system (HTX; BioTek) to determine the viability of the MT.

Statistical analysis: All measurements were performed three times per experiment. Quantitative data are presented as means ± standard error. The data were analyzed using SigmaPlot 12 (Systat Software, Richmond, CA, USA). Student's *t*-test was used for the analysis and $p < 0.05$ was taken to indicate statistical significance.

Acknowledgments

We thank the CCRF of DGIST for technical support. The authors are also grateful to Jiyoun Park (DGIST) for technical support of SEM inspection, Sungki Jeon, Byungmok Sung (DGIST) for help of 3D laser lithography and sputtering system, and Eungjung Shin, Chaewon Jin (DGIST) for technical support of design and cell-culture. Funding for this research was

provided by the Global Research Laboratory from the National Research Foundation of Korea (NRF) and by the DGIST R&D Program, funded by the Ministry of Science, ICT & Future Planning (NO. NRF 2017K1A1A2013237 and 19-CoE-BT-02).

References

[1] R. K. Portenoy, P. Lesage, *Lancet* **1999**, 353, 1695.
[2] E. Kawabata-Shoda, S. Masuda, H. Kimura, *J. Clin. Pharm. Ther.* **2012**, 37, 547.
[3] R. B. S, S. S. Narayan, G. R. K. Sharma, R. J. Rodrigues, C. Kulkarni, *Pharmacoepidemiol. Drug Saf.* **2008**, 17, 807.
[4] a) A. Servant, F. Qiu, M. Mazza, K. Kostarelos, B. J. Nelson, *Adv. Mater.* **2015**, 27, 2981; b) F. Qiu, L. Zhang, K. E. Peyer, M. Casarosa, A. Franco-Obregon, H. Choi, B. J. Nelson, *J. Mater. Chem. B* **2014**, 2, 357; c) F. Qiu, R. Mhanna, L. Zhang, Y. Ding, S. Fujita, B. J. Nelson, *Sens. Actuators, B* **2014**, 196, 676; d) F. Qiu, S. Fujita, R. Mhanna, L. Zhang, B. R. Simona, B. J. Nelson, *Adv. Funct. Mater.* **2015**, 25, 1666; e) R. Mhanna, F. M. Qiu, L. Zhang, Y. Ding, K. Sugihara, M. Zenobi-Wong, B. J. Nelson, *Small* **2014**, 10, 1953; f) A. Ghosh, P. Fischer, *Nano Lett.* **2009**, 9, 2243; g) J. Park, C. Jin, S. Lee, J.-Y. Kim, H. Choi, *Adv. Healthcare Mater.* **2019**, 8, 1900213.
[5] a) Kim, F. Qiu, S. Kim, A. Ghanbari, C. Moon, L. Zhang, B. J. Nelson, H. Choi, *Adv. Mater.* **2013**, 25, 5863; b) H. Choi, S. Kim, S. Lee (DGIST), US 10,485,648 B2, **2019**
[6] S. Kim, S. Lee, J. Lee, B. J. Nelson, L. Zhang, H. Choi, *Sci. Rep.* **2016**, 6, 30713.
[7] a) S. Lee, S. Kim, S. Kim, J.-Y. Kim, C. Moon, B. J. Nelson, H. Choi, *Adv. Healthcare Mater.* **2018**, DOI: 10.1002/adhm.2017009851700985; b) H. Choi, S. Kim, S. Lee (DGIST), US 10,188,841 B2, **2019**
[8] M. Medina-Sánchez, L. Schwarz, A. K. Meyer, F. Hebenstreit, O. G. Schmidt, *Nano Lett.* **2016**, 16, 555.
[9] a) C. Peters, M. Hoop, S. Pané, B. J. Nelson, C. Hierold, *Adv. Mater.* **2015**, 28, 533; b) H. Ceylan, I. Yasa, Ö. Yaşa, A. F. Tabak, J. Giltinan, M. Sitti, *ACS Nano* **2018**, 13, 3353; c) O. Felfoul, M. Mohammadi, S. Taherkhani, D. de Lanauze, Y. Zhong Xu, D. Loghin, S. Essa, S. Jancik, D. Houle, M. Lafleur, L. Gaboury, M. Tabrizian, N. Kaou, M. Atkin, T. Vuong, G. Batist, N. Beauchemin, D. Radzioch, S. Martel, *Nat. Nanotechnol.* **2016**, 11, 941; d) K. Malachowski, J. Breger, H. R. Kwag, M. O. Wang, J. P. Fisher, F. M. Selaru, D. H. Gracias, *Angew. Chem., Int. Ed. Engl.* **2014**, 53, 8045; e) A. Abramson, E. Caffarel-Salvador, M. Khang, D. Dellal, D. Silverstein, Y. Gao, M. R. Frederiksen, A. Vegge, F. Hubálek, J. J. Water, A. V. Friderichsen, J. Fels, R. K. Kirk, C. Cleveland, J. Collins, S. Tamang, A. Hayward, T. Landh, S. T. Buckley, N. Roxhed, U. Rahbek, R. Langer, G. Traverso, *Science* **2019**, 363, 611.
[10] a) F. Ullrich, C. Bergeles, J. Pokki, O. Ergeneman, S. Erni, G. Chatzipirpiridis, S. Pane, C. Framme, B. J. Nelson, *Invest Ophthalmol Vis Sci* **2013**, 54, 2853; b) S. K. Srivastava, M. Medina-Sánchez, B. Koch, O. G. Schmidt, *Adv. Mater.* **2016**, 28, 832; c) C. Forbrigger, A. Lim, O. Onaizah, S. Salmanipour, T. Looi, J. Drake, E. D. Diller, *IEEE Trans. Robot. Autom.* **2019**, 4, 1202.
[11] a) O. Ergeneman, G. Chatzipirpiridis, J. Pokki, M. Marin-Suarez, G. A. Sotiriou, S. Medina-Rodriguez, J. F. Sanchez, A. Fernandez-Gutierrez, S. Pane, B. J. Nelson, *IEEE Trans Biomed Eng* **2012**, 59, 3104; b) W. Jing, S. Chowdhury, M. Guix, J. Wang, Z.

An, B. V. Johnson, D. Cappelleri, *IEEE Trans. Autom. Sci. Eng.* **2018**, DOI: 10.1109/TASE.2018.28338101.

[12] F. Ullrich, K. S. Dheman, S. Schuerle, B. J. Nelson, *IEEE Int Conf Robot Autom*. **2015**, DOI: 10.1109/ICRA.2015.71394241751.

[13] H. Lai, N. P. Singh, *Environ Health Perspect* **2004**, 112, 687.

[14] B. J. Nelson, I. K. Kaliakatsos, J. J. Abbott, *Annu Rev Biomed Eng* **2010**, 12, 55.

[15] B. E. Kratochvil, M. P. Kummer, S. Erni, R. Borer, D. R. Frutiger, S. Schürle, B. J. Nelson, in *Experimental Robotics: The 12th International Symposium on Experimental Robotics*, DOI: 10.1007/978-3-642-28572-1_22, Springer Berlin Heidelberg, Berlin, Heidelberg **2014**, p. 317.

[16] A. W. Mahoney, N. D. Nelson, K. E. Peyer, B. J. Nelson, J. J. Abbott, *Appl. Phys. Lett.* **2014**, 104, 144101.

[17] a) K. L. Johnson, K. L. Johnson, *Contact mechanics*, Cambridge university press, **1987**; b) K.-C. Wu, H.-I. You, *Appl. Surf. Sci.* **2007**, 253, 8530; c) M. H. Korayem, Z. Mahmoodi, M. Taheri, M. Saraee, *Proceedings of the Institution of Mechanical Engineers, Part K: Journal of Multi-body Dynamics* **2015**, 229, 370.

[18] a) J. Kim, H. Choi, J. Kim, *IEEE-ASME T MECH.* **2019**, DOI: 10.1109/TMECH.2019.29071451; b) A. Ghanbari, P. H. Chang, B. J. Nelson, H. Choi, *INT J OPTOMECHATRONI.* **2014**, 8, 129; c) A. Ghanbari, P. H. Chang, B. J. Nelson, H. Choi, *Smart Mater. Struct* **2014**, 23, 035013.

[19] D. Mastropaolo, A. Camerman, Y. Luo, G. D. Brayer, N. Camerman, *Proc Natl Acad Sci U S A* **1995**, 92, 6920.

Figure Legends

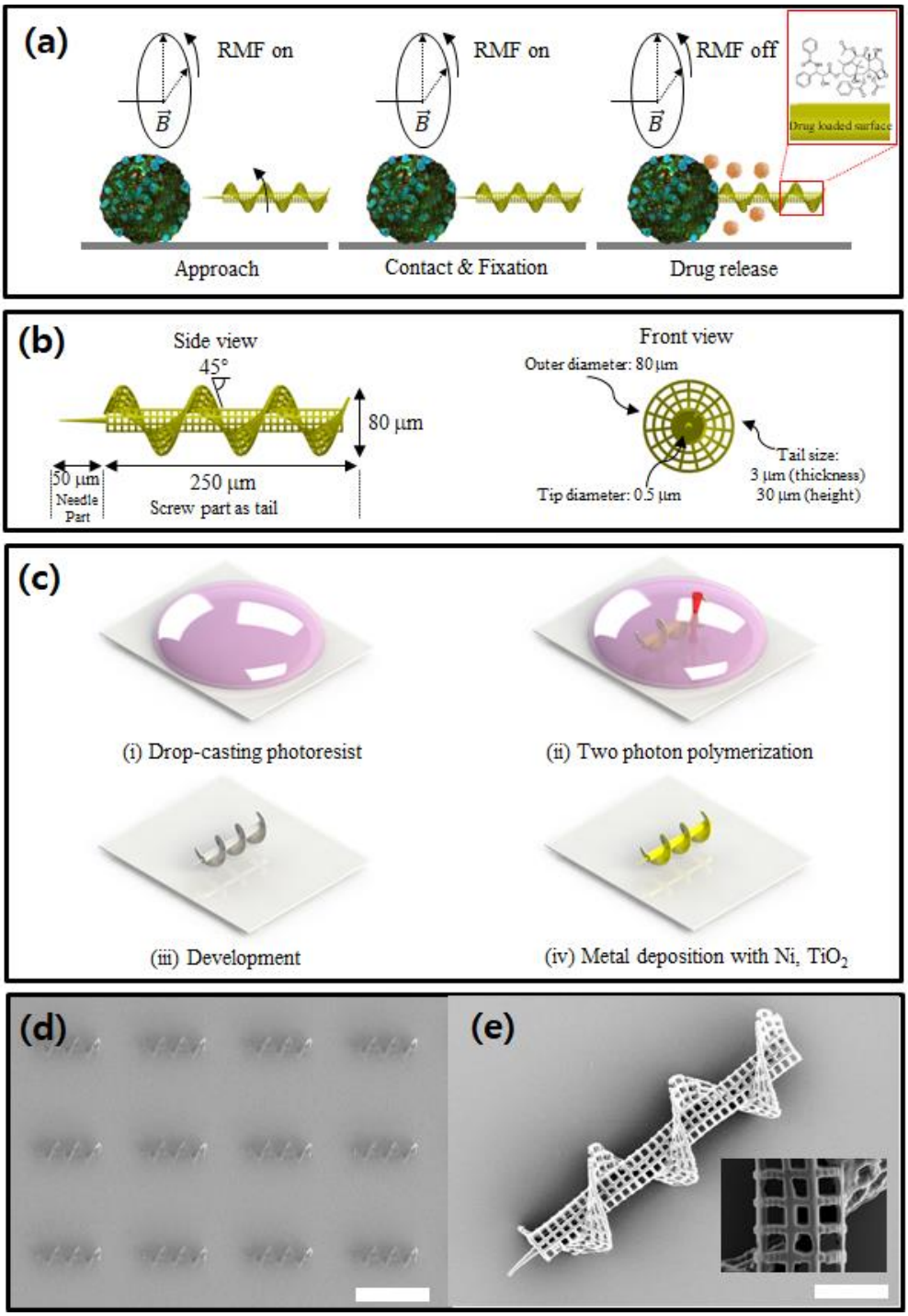

Figure 1. (a) Drug release method of the proposed MR. (b) Dimensions of the MR. (c) Fabrication procedure of the needle-type MR using two-photon polymerization and physical vapor deposition. (d, e) SEM images of the fabricated MRs. Scale bars: 300 μm in Figure (d), 40 μm in Figure (e)

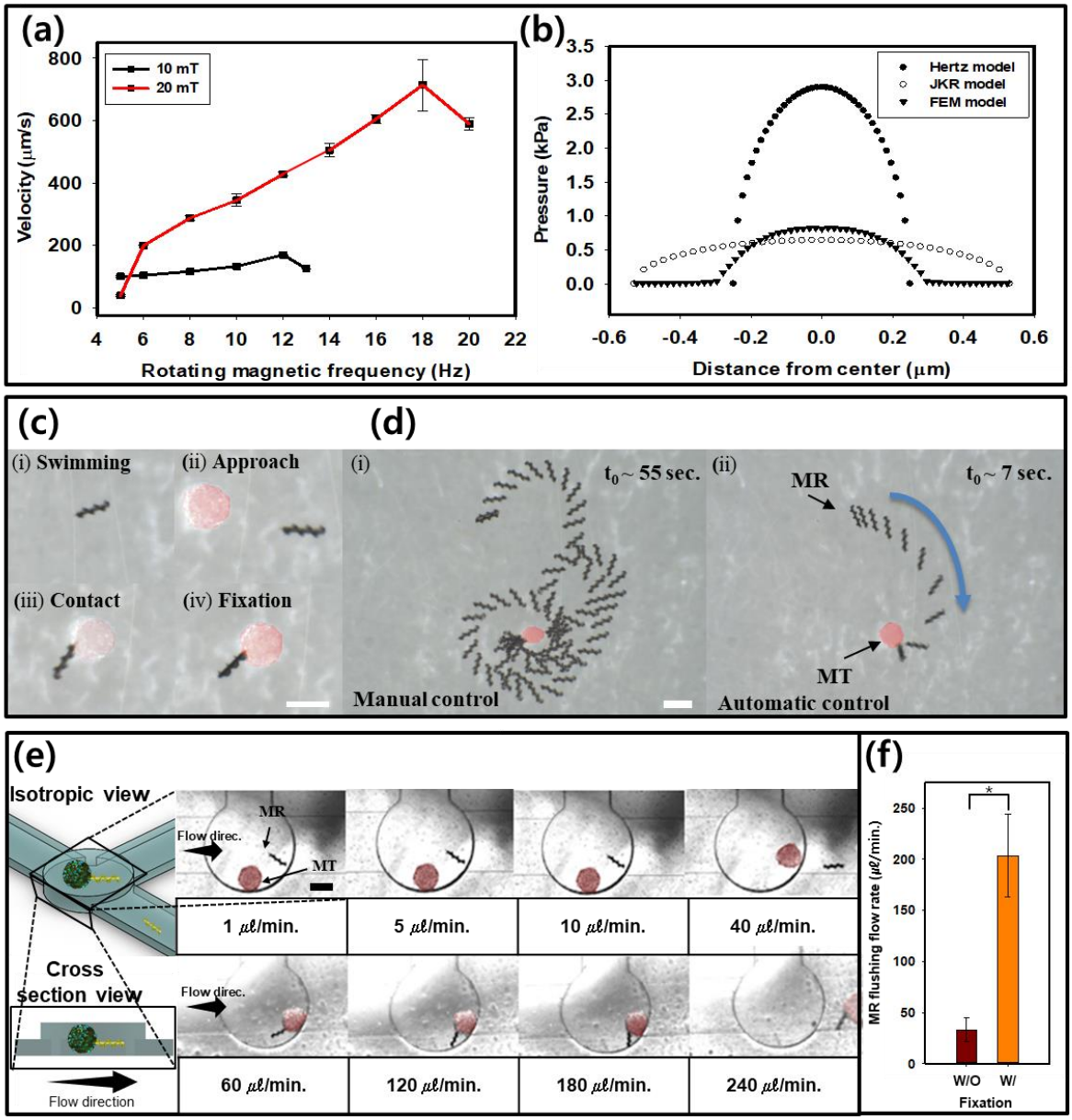

Figure 2. (a) Translational velocity of the needle-type MR. (b) Distribution of contact pressure calculated by theoretical and FE models. (c) Procedure for affixing the MR to the HCT116 MT: swimming, approach, contact, and fixation. (d) Time-lapse images of a swimming MR under manual and automatic control. (e) Results of flow resistance experiments. (f) Flow rate until the MR was flushed away from the HCT116 MT before and after fixation. *$p < 0.05$, $n = 3$. F. R., flow rate. Scale bar: 300 μm.

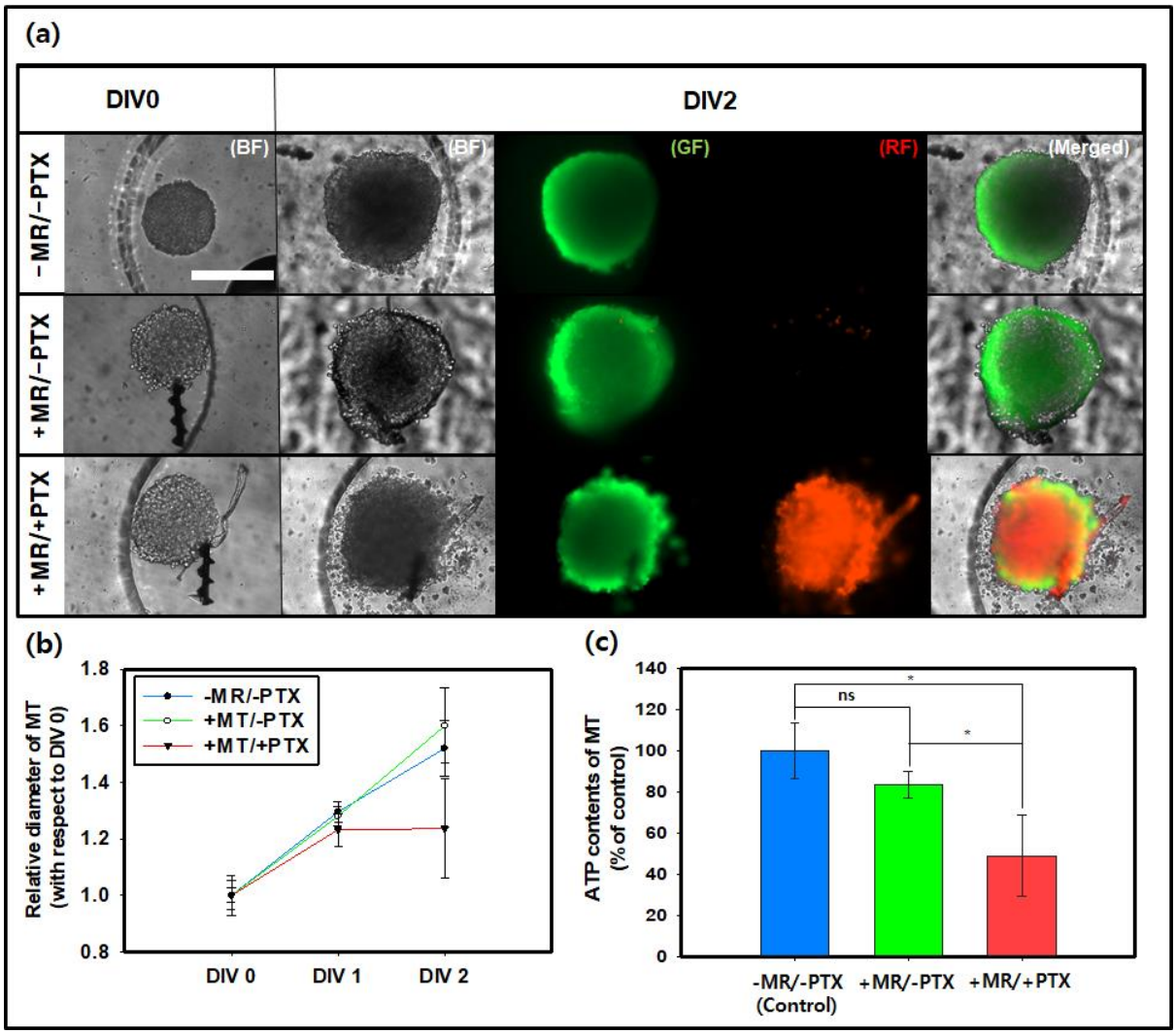

Figure 3. (a) Bright-field and fluorescence images of the HCT116 MTs under perfusion conditions in a gravity flow system at DIV0 and 2. (b) Relative diameter of the MT at DIV2. (c) ATP contents of the HCT116 MTs. Results are presented as means ± standard deviation (*$p < 0.05$; ns, $p > 0.05$; $n = 3$). MR, microrobot. Scale bar: 300 μm.

Table of Contents (TOC):

A needle-type microrobot was fabricated by 3D laser lithography for stable durg delivery. The durg-loaded microrobot can be fixed to a target microtissue by swimming in a corkscrew motion with magnetic torque under a rotating magnetic field. The results demonstrated the potential of the needle-type microrobot to improve targeted drug delivery to microtissue with various flow rates in vitro physiological fluidic environments.

Keywords: Microrobot; magnetic manipulation; drug delivery; targeted delivery; fixation

*Seungmin Lee, Jin-young Kim, Junyoung Kim, Ali Kafash Hoshiar, Jongeon Park, Sunkey Lee, Jonghyun Kim, Salvador Pané, Bradley J. Nelson, and Hongsoo Choi**

Title: A needle-type microrobot for targeted drug delivery by affixing to a microtissue